Long TiO_2 Hollow Fibers with Mesoporous Walls: Sol−Gel Combined Electrospun Fabrication and Photocatalytic Properties

Sihui Zhan, Dairong Chen,* Xiuling Jiao, and Caihong Tao

Department of Chemistry, Shandong University, Jinan 250100, P R China

Received: December 18, 2005; In Final Form: April 9, 2006

Long TiO_2 hollow fibers with mesoporous walls have been fabricated with the sol−gel combined two-capillary spinneret electrospinning technique using a triblock copolymer (Pluronic, P123, $(H(C_2H_5O)_{20}(C_3H_7O)_{70}(C_2H_5O)_{20}OH)$ as a pore-directing agent. The as-prepared hollow fibers were as long as 30 cm with an outer diameter of 0.1−4 μm and wall thickness of 60−500 nm. The diameters and wall thicknesses of the hollow fibers could be tuned by adjusting the electrospinning parameters. The fiber walls were composed of mesopores 6.7 nm in diameter as calculated from the N_2 adsorption/desorption isotherm. The high-resolution TEM (HR-TEM) images exhibited that the mesopores were hexagonally aligned with a low order because of the curving of the pores. When comparing with other nanostructured TiO_2 materials such as commercial TiO_2 nanoparticles (P25, Degussa) and mesoporous TiO_2 powders, the hollow fibers exhibited higher photocatalytic activities toward degradation of methylene blue and gaseous formaldehyde.

1. Introduction

Titania (TiO_2) is a typical n-type semiconductor and widely used photocatalyst, with excellent catalytic properties for the elimination of pollutants in gas or liquid phases. Nanostructured TiO_2 exhibits superior photocatalytic activity compared to conventional bulk materials because of its high surface area and is one of the most intensively researched substances of the past decade.[1] To enhance its photocatalytic ability, various morphologies of nanostructured TiO_2 including nanoparticles, nanofibers, nanostructured films or coatings, nanotubes, and so forth have been prepared, and much progress on the synthesis of nanostructured TiO_2 with excellent catalytic properties has been made.[2−4] However, application of these nanostructured TiO_2 materials, especially in purification of water, is challenging. For practical applications as a photocatalyst, a material must have superior catalytic activity and be easily synthesized, fixed, and reclaimed. Use of microspheres/tubes and nanotubes/fibers might repollute the water unless they can be fixed and reclaimed. The nanofilms can be fixed, but have so far been fabricated through tedious and costly processes. To improve the properties of TiO_2 for potential applications in photocatalysis and other areas, Peng and co-workers described a sol−gel method to fabricate TiO_2 microtubules with mesoporous walls in a laurylamine hydrochloride/tetra-*n*-butylorthotitanate system.[5] Mukai et al.[6] prepared porous TiO_2 cryogel fibers with a length of several micrometers through unidirectional freezing and subsequent freeze-drying of TiO_2 hydrogels. Caruso et al.[7] fabricated long TiO_2 hollow fibers with porous walls by coating electrospun organic fibers. Recently, Loscertales's group[8] and Xia et al.[9] independently prepared inorganic (SiO_2 and TiO_2) hollow fibers by co-electrospinning an aged inorganic sol and an immiscible (or poorly miscible) liquid such as olive (mineral) oil or glycerin, followed by selective removal of the oil by extraction and calcination. The resultant hollow fibers had a mean inner diameter in the submicroscale, length in the centimeters, and dense walls.

In this paper, TiO_2 hollow fibers as long as 30 cm with mesoporous walls are introduced. These TiO_2 hollow fibers, which can be prepared on a large scale, have large surface areas and exhibit superior catalytic properties, and as long fibers, the mesoporous TiO_2 can be fixed and reclaimed easily.

In the past decade, hollow inorganic fibers or tubules with mesoporous walls have attracted much attention for their structural particularity. The hierarchical tubules-within-a-tubule structure was important for its technological promise in applications such as catalysis, selective separation, sensor arrays, waveguides, miniaturized electronic and magnetic devices, and photonic crystals with tunable band gaps.[10] In addition, it could act as a minitype reactor, has potential applications in nanotechnology, and the long hollow fibers could be expediently operated and reclaimed. Mou's group first reported the synthesis of MCM-41 tubules through a membrane-to-tubule transformation in highly alkaline solution.[11] Since then, there have been many reports on tubular mesoporous materials, and several fabrication methods have been proposed, which can be classified into two types: hard-template synthesis and self-assembly.[12] The hard-template process proved to be an effective approach to producing hollow tubules, but the resultant material was limited by the morphology and structure of the templates. Using self-assembly techniques, mesoporous tubules with dimensions from nano- to micrometers have been prepared, and their morphology is usually determined by the cooperative organization of inorganic and organic species. However, the length of the obtained tubules is usually in the micro- or submicroscale, and the formation of tubular structures was always incidental.[13] Although great improvements have been made on the preparation of inorganic fibers with mesoporous or hollow structures,[14] the fabrication of inorganic hollow fibers with mesoporous walls and lengths of centimeters has not been reported previously, to the best of our knowledge.

As a simple and convenient method, electrospinning processes[15] have been investigated for preparing long nanofibers

* Corresponding author. Tel: +86-0531-88364280. Fax: +86-0531-88364281. E-mail: cdr@sdu.edu.cn.

10.1021/jp057372k CCC: $33.50
Published on Web 05/25/2006

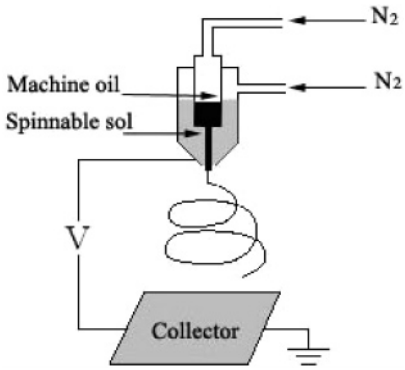

Figure 1. Diagram of the co-electrospinning apparatus.

of polymers, ceramics, carbons, and composites,[16] and enormous efforts have been made to improve electrospinning for use in other applications.[17] Since the co-electrospinning process was first introduced by Loscertales's group[8] and Greiner et al.,[18] there have been many reports on the fabrication of core−shell fibers and hollow fibers including organic polymers and inorganic fibers. In the present work, the fabrication of the TiO_2 hollow fibers by co-electrospinning an aged inorganic sol and an immiscible liquid provided a new route to the production of inorganic hollow fibers with mesoporous walls. In addition, it may enrich the co-electrospinning techniques for preparation of nanostructured materials with new morphologies.

2. Experimental Section

2.1. Synthesis. Hydrochloric acid (36.0 wt %), titanium *n*-butyloxide ($Ti(OC_4H_9^n)_4$), Pluronic P123 (M_w = 5800, containing 30.0 wt % ethylene glycol monomer), and ethanol (>99.7%) were all analytical grade and were used as received without further purification. The precursor sol for electrospinning was prepared according to ref 17a. In a typical synthesis, 1.48 mmol P123 was dissolved in 20.0 mL absolute ethanol, and 40.0 mmol $Ti(OC_4H_9^n)_4$ was added into the mixture of 10.0 mL ethanol and 2.0 mL concentrated HCl. The two solutions were mixed at room temperature, then transferred into a 250 mL three-orifice flask under N_2 atmosphere, and aged at 45 °C for 16 h to give a spinnable sol.

As shown in Figure 1, the spinnable sol was added into the outer tube, and machine oil was poured into the inner capillary. The outer tube and inner capillary were made of stainless steel, and the two fluids were pressurized with N_2 to drive the fluid to the tip of the spinneret, which was connected to a high-voltage supply (BGG-200 kV/20 mA). With the adjustment of the oil and sol pressures, hollow fibers with tunable inner diameters and wall thicknesses were obtained. During the electrospinning process, the applied voltage was 25 kV, the distance between spinneret and collector was 30 cm, and the temperature was maintained at 22 °C. After the collected fibers were soaked in cyclohexane for 24 h to thoroughly extract the machine oil and dried at room temperature for 24 h, xerogel hollow fibers were obtained.

The xerogel hollow fibers were heated at 130 °C for 8 h and calcined at 400 °C for 4 h in air at a heating rate of 0.5 °C·min^{-1} from 130 °C to 400 °C to completely eliminate the organics. After cooling to room temperature, mesoporous TiO_2 hollow fibers were obtained.

2.2. Characterization. The rheology and viscoelasticity of the sol were measured on a RS75 Rheometer (HAAKE Co.) at room temperature. The morphology and structure of the fibers were observed by use of a scanning electron microscope (SEM, Hitachi S-520, JXA-840). The low-angle X-ray diffraction (LA-XRD) patterns of the samples were recorded on an X-ray diffractometer (Rigaku D/Max 2200PC) with a graphite monochromator and Cu Kα radiation (λ = 0.15418 nm) in the range of 0.7−5° at room temperature while the voltage and electric current were held at 28 kV and 20 mA. The XRD patterns of the samples were applied to identify the phase of fibers, and the voltage and electric current were maintained at 40 kV and 20 mA (2θ = 10−75°). The infrared (IR) spectra were recorded on a Nicolet 5DX-FTIR spectrometer using the KBr pellet method in the range of 400−4000 cm^{-1}. A high-resolution transmission electron microscopy (HR-TEM, GEOL-2010) was used to characterize the microstructure of the fibers, where the samples were microtomed into thin slices and transferred onto carbon grids. Thermal gravimetric (TG) analysis was employed to evaluate the weight loss of the samples under air flow of 20 mL·min^{-1} and a heating rate of 20 °C·min^{-1} using a thermal analyzer (TGA/SDTA, 851^e METTLER). N_2 adsorption−desorption data were determined using a Coulter 100CX micromeritics apparatus, and the isotherms were evaluated with the Barrett−Joyner−Halenda (BJH) theory to give the surface area, pore size, and pore distribution.

2.3. Photocatalytic Activity Measurements. The photocatalytic activities of the mesoporous TiO_2 hollow fibers on the photooxidation of methylene blue were investigated first.[19] Deionized water was used as a blank. The sample with the weight of 1.0 mg was added to 100.0 mL methylene blue solution with a concentration of 2.0 mg/L, and the solution was irradiated by a 125 W high-pressure mercury lamp (λ = 320−400 nm, λ_{max} = 365 nm) with stirring. The change of absorption at 664 nm was applied to identify the concentration of methylene blue using an UV−vis spectrophotometer (Lambda 35, Perkin-Elmer), and the concentration of methylene blue was measured as a function of irradiation time.

The photodecomposition of formaldehyde gas was also studied using the prepared hollow fiber as photocatalyst. The sample with the weight of 1.0 mg was placed into a 250.0 mL glass bottle and filled with gaseous formaldehyde by vaporization of 5 μL 37% formaldehyde solution in air to produce an initial concentration of formaldehyde of 8.36 g/m^3.[20,21] After the gas−solid adsorption process reached equilibrium (1 h in the absence of light), the photoreactor bottle was irradiated with the mercury lamp, and the phenol-spectrophotometry method (Chinese Criterion GB/T 18204.26−2000) was applied to determine the concentration change of gaseous formaldehyde at different UV irradiation times.

3. Results and Discussion

3.1. Fabrication of TiO_2 Hollow Fibers. The Pluronic (P123, $H(C_2H_5O)_{20}(C_3H_7O)_{70}(C_2H_5O)_{20}$−OH) was used as a pore-directing agent, titanium *n*-butyloxide was used as the Ti source, and ethanol was used as the solvent to prepare the spinnable sol. In the electrospinning process (Figure 1),[15,16] the sol was elongated, of which solvent volatilizing, to form the core−shell structured fibers. After the fibers were extracted by use of cyclohexane to eliminate the machine oil (core) and dried at room temperature, the hollow xerogel fibers were obtained. From the optical photograph of the gel fibers (Supporting Information Figure S1a), it was found that the gel fibers were as long as 30 cm, and they interlinked to form a large nonwoven web. The SEM image (Figure S1b) showed that these hollow xerogel fibers had uniform diameters of 1−4 μm and lengths of several centimeters.

The spinnable sol was important for the preparation of the fibers, whose rheological properties determined the morphology

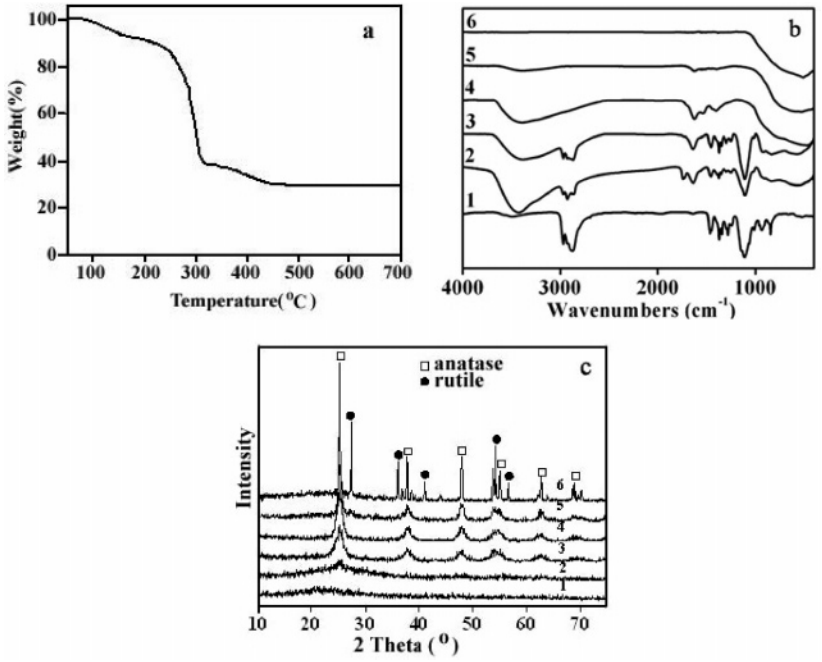

Figure 2. (a) TG curve of the TiO_2 xerogel fibers; (b) IR spectra of Pluronic P123 (1), the xerogel fibers (2), and those calcined at different temperatures: (3) 200 °C, (4) 320 °C, (5) 400 °C, and (6) 800 °C for 4 h in air; (c) XRD patterns of the xerogel hollow fibers before (1) and after calcination at (2) 200 °C, (3) 320 °C, (4) 400 °C, (5) 600 °C, and (6) 800 °C for 4 h in air.

and diameter of the xerogel fibers. Lower viscosity of the spinnable sol always results in the formation of thinner fibers. In the present work, the rheological curve of the precursor sol exhibited the characteristics of a Newtonian fluid, indicating its spinnability (Supporting Information, Figure S2). When the aging time was prolonged, its viscosity increased significantly. The experiments demonstrated that the viscosity was too small to electrospin when the aging time was less than 14 h. When the aging time was more than 17 h, the sol behaved as a non-Newtonian fluid and was difficult to use to prepare the hollow fibers. The formation of mesostructured materials by the sol−gel process requires rigorous conditions, that is, control of the pH value, sol composition, evaporation condition, and rheological properties of the sol.[22] The viscosity range of the spinnable sol for electrospun fibers is broad, and that for the mesostructural materials is narrow. On the basis of the results of a series of experiments, the optimal viscosity of the precursor sol was 4−7 Pa·S corresponding to an aging time from 15 to 16 h, which was much smaller than the viscosity of sols employed in a mechanical spinning process.[23] And the optimal mesostructure was obtained when the solvent evaporates at a relative humidity (RH) of ca. 45% and a temperature of 25 °C.

In the present work, when the other parameters were kept as described in the Experimental Section, TiO_2 hollow fibers with tunable diameters and wall thicknesses were obtained by adjusting the sol and oil pressures. When the sol and oil pressures were all 0.1 MPa, the wall thickness of the hollow fibers was ca. 300 nm and the outer diameters of the fibers ranged from 2 μm to 4 μm. When the inner and outer pressures were decreased to 0.05 MPa, the diameter of the hollow fibers was ca. 450 nm, with wall thicknesses of ca. 150 nm. When the oil and sol pressure were maintained at 0.05 and 0.02 MPa, respectively, the outer diameter of the fibers was 250−400 nm and the wall thickness was only 100 nm (Supporting Information, Figure S3c). Increasing the oil pressure to 0.15 MPa and maintaining the sol pressure at 0.05 MPa decreased the wall thickness to ca. 60 nm. This result indicates that higher oil pressure promotes formation of hollow fibers with thinner walls, whereas higher sol pressure produces hollow fibers with thicker walls. The diameter and wall thickness of the TiO_2 fibers were determined by the oil and sol pressures or their ratio. The BET surface areas of the above three samples were 200 m^2/g, 206 m^2/g, and 208 m^2/g, respectively. The similar surface areas of the calcined TiO_2 fibers indicated that most of the surface area could be attributed to the mesopores in the walls and that the outer and inner walls of the hollow fibers contributed much less to the total surface area than the mesoporous channels.

The TG curve (Figure 2a) of the xerogel fibers shows three steps and a total weight loss of ca. 72.0%. The first step of ca. 9.0% from 60 to 200 °C could be attributed to the desorption of water, and the second significant weight loss of ca. 54% between 200 and 320 °C was assigned to the decomposition of the P123 template in the nanochannels of the microtubule walls. From 320 to 440 °C, there was a weight loss of ca. 9.0%, which was assigned to the removal of water molecules from the hydroxyls on titanium atoms and a small amount of residual organic material. These results show that the organic template was removable from the fibers upon calcination at 440 °C. Above 440 °C, there was no further weight loss, which indicated that the organic component had been entirely decomposed. The IR spectra of the xerogel fibers and those calcined at different temperatures (Figure 2b) confirmed the above results. The IR spectrum of the xerogel fibers showed a strong adsorption around 3400 cm^{-1}, which was assigned to the hydroxyls from water, P123, and Ti−OH, and the weak peak at 1720 cm^{-1} also indicated the presence of water. The adsorption peaks from 1520 to 1432 cm^{-1} were attributed to C−H vibrations of hydrocarbons in the xerogel fibers. The shift from 3500 cm^{-1} corresponded to the hydroxyls of pure P123 to 3400 cm^{-1} also demonstrated that P123 hydrogen-bonded to Ti−OH. After the xerogel fibers were calcined at 200 °C for 4 h in air, the strong absorptions around 3400 cm^{-1} weakened significantly. After calcination at 400 °C, the peaks from 1520 to 1432 cm^{-1} almost disappeared, indicating the complete removal of P123, and absorptions around 530 cm^{-1} appeared, which are attributed to the Ti−O vibrations of anatase TiO_2. The XRD patterns (Figure 2c) indicated that the xerogel fibers began to crystallize at 200 °C, and the anatase TiO_2 walls were formed after calcination at 320 °C. The intensity

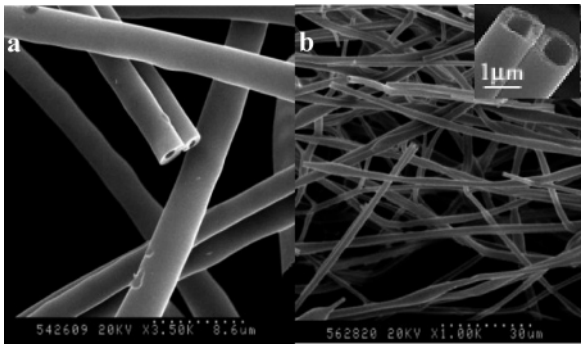

Figure 3. SEM images of the xerogel (a) and TiO_2 (b) hollow fibers. All of the sol and oil pressures were 0.1 MPa.

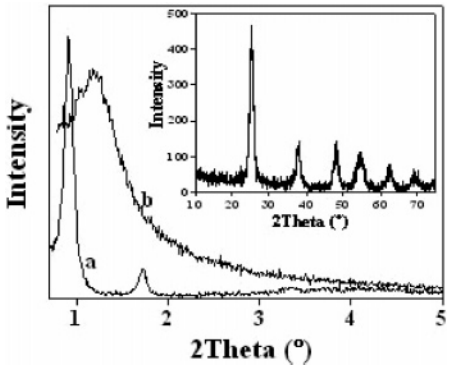

Figure 4. LA-XRD patterns of xerogel (a) and TiO_2 (b) hollow fibers. The inset shows the XRD pattern of the hollow fibers after calcination at 400 °C for 4 h in air.

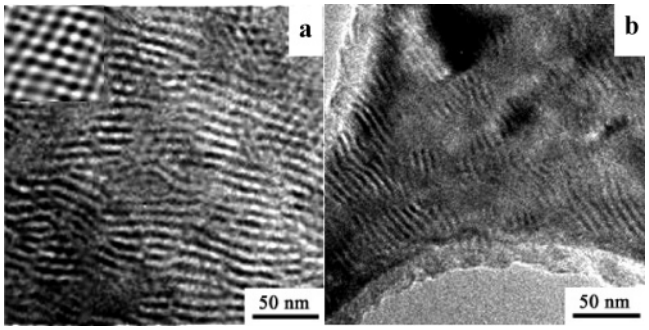

Figure 5. HR-TEM images of cross sections of TiO_2 hollow fibers calcined at 400 °C for 4 h in air (a) perpendicular to the axis and (b) parallel to the axis.

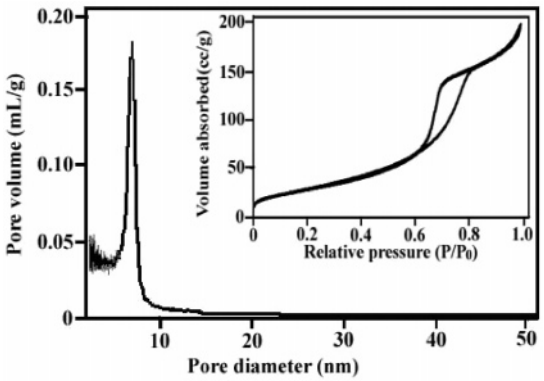

Figure 6. N_2 adsorption−desorption isotherm (inset) and the calculated pore size distribution of TiO_2 hollow fibers.

of the reflections corresponding to the anatase structure increased as the calcination temperature increased from 320 to 600 °C. When the xerogel fibers were calcined at 400 °C for 4 h, the mean size of anatase TiO_2 nanocrystals was ca. 10 nm based on the Scherrer equation. After the xerogel fibers were heat-treated at 600 °C, the Bragg peaks became higher and sharper, indicating increased particle sizes. Furthermore, it was found that the mesopores shrank quickly as the temperature increased, and the rutile structure formed and mesopores disappeared after the xerogel fibers were calcined at 800 °C, according to the LA-XRD pattern and HR-TEM images.

3.2. Microstructure of TiO_2 Hollow Fibers. The SEM images of the typical xerogel and TiO_2 fibers in Figure 3 show that they are hollow tubes with open ends. The cross section of the hollow fibers demonstrated that the wall thickness was uniform. The xerogel fibers had a wall thickness of ca. 500 nm, smooth surfaces, and outer diameters ranging from 3 to 4 μm (Figure 3a). The outer surface of the TiO_2 hollow fibers was much coarser than the xerogel fibers, although the TiO_2 fibers still retained their tubular form without cracking. The TiO_2 hollow fibers had wall thicknesses of ca. 300 nm and their outer diameters decreased to 2−4 μm as a result of calcination (Figure 3b), which demonstrated that the xerogel fibers shrank with the removal of organics.

The LA-XRD pattern of the xerogel fibers (Figure 4) showed a strong, sharp peak centered at $2\theta = 0.9°$ corresponding to a *d* spacing of 9.9 nm and a relative lower peak. According to their *d* spacings, the peaks can be indexed to (100) and (200) reflections. The HRTEM observation indicates the 2D hexaganol mesostructure, indicating that the (110) reflection cannot be detected in the present LAXRD pattern, which is similar to previous reports.[24a,b] The absence of the (110) reflection is due to the orientation of the xerogel fibers during XRD analysis, which exhibits as a nonwoven cloth and seems to be a thick film (Supporting Information, Figure S4). To further confirm this point, the XRD pattern of the xerogel fibers was recorded after the fibers were ground into powder to avoid the orientation during the XRD analysis. As expected, the LA-XRD pattern exhibited three reflections, which were indexed to (100), (110), and (200) reflections of the hexagonal structured material (Supporting Information, Figure S5). After calcination, this peak shifted to 1.2°, corresponding to a *d* value of 7.5 nm, with decreased intensity and broadening. According to previous reports and the observation from HRTEM image, it is concluded the broad peak at 1.2° results from the average pore-to-pore separation but not the order arrangement of the mesostructure, which is like that observed from mesoporous material with wormhole-like pores.[4c,24d,25,30a] The HRTEM image clearly indicates the poor order of the pores, although the 2D hexagonal structure can be seen in some area, which results from the collapsing of pores during calcinations.[24,25] The XRD pattern showed that anatase TiO_2 was formed after the xerogel fibers were calcined at 400 °C for 4 h (Figure 4, inset), and the mean size of the anatase TiO_2 nanocrystals was ca. 10 nm, as calculated by the Scherrer equation.[24c,26a] The well-resolved XRD peaks attributed to the anatase TiO_2 phase indicated the highly crystalline nature of the mesoporous framework, which is similar to previous reports. [24−26,31a]

The HR-TEM images (Figure 5) show that the pores exhibited hexagonal alignment with a few disturbances in the thicker region viewing from the direction perpendicular to the fiber axis, and the pore size ranged from 6 to 7 nm after calcining these hollow fibers at 400 °C for 4 h in air.[27] The arrangements of most nanochannels from the cross section of TiO_2 fibers were out of order, and some pore channels exhibited hexagonal ordering (Figure 5a, inset), which was different from the mesoporous TiO_2 solid fibers prepared by Madhugiri et al. in which the obtained TiO_2 fibers had wormlike pores.[17a] The

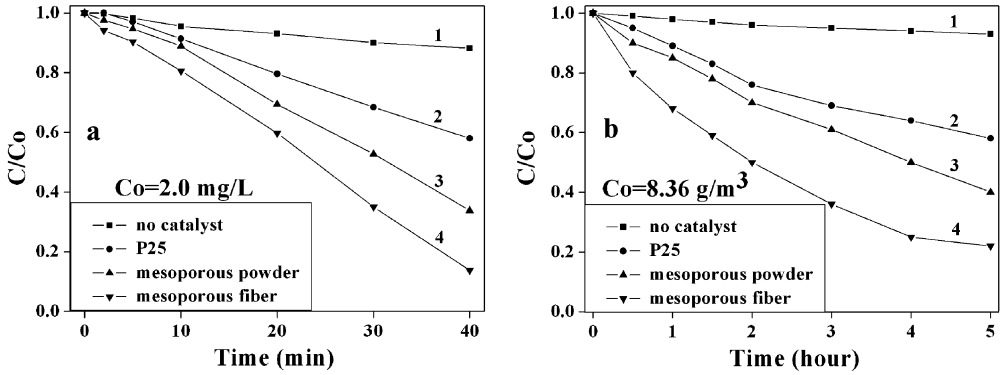

Figure 7. Time courses for UV photodegradation of methylene blue (a), and gaseous formaldehyde (b). Curves: (1) without photocatalyst, (2) commercial P25 (BET surface area: 50 m^2/g, mean size: 20 nm, phase: anatase/rutile = 80/20), (3) mesoporous powders (BET surface area: 167 m^2/g, the pore size was the same as that of the hollow fibers), (4) mesoporous hollow fibers (BET surface area: 208 m^2/g).

difference might be due to the short aging time of the precursor sol or the effect of the electric field in the present experiment.

The N_2 adsorption−desorption isotherm of the TiO_2 hollow fiber (Figure 6, inset) shows a type IV-like isotherm with a sharp increase of the adsorbed volume at $P/P_0 = 0.63$, indicating the presence of well-developed mesopores in the walls of the TiO_2 hollow fibers. The pore size distribution was calculated based on BJH (Barrett−Joyner−Halenda) theory. From the adsorption branch of the isotherm, there is a narrow pore-size distribution with an average pore size of 6.7 nm, which was in accordance with the sizes observed by HR-TEM (Figure 5). The BET surface area and specific pore volume of the sample were 208 m^2/g and 48.0 cm^3/g, respectively.

3.3. Photocatalytic Activity. The photocatalytic activity of TiO_2 is determined primarily by its physicochemical properties such as morphology, particle size, surface area, and porosity.[28,29] The photocatalytic properties of the mesoporous TiO_2 hollow fibers were evaluated by photo-oxidation of methylene blue.[19] The prepared mesoporous TiO_2 powder composed of anatase TiO_2 was used to investigate the effect of the morphology on the photocatalytic activity. At the same time, the commercially available photocatalyst P25 (Degussa),[1a,17a,24c] which is a mixture of anatase and rutile forms in the ratio of 4:1, was also used as reference because of its high photocatalytic activity.[30] The adsorption of methylene blue at 664 nm almost disappeared, and the blue color of the solution vanished completely after the methylene blue solution was irradiated for 40 min in the presence of TiO_2 hollow fibers (Supporting Information, Figure S6). Figure 7a shows the photocatalytic activities of the mesoporous TiO_2 hollow fibers evaluated by degradation of methylene blue (curve 4). As a comparison, the photodegradation in the absence of photocatalyst (curve 1), and with commercial photocatalyst Degussa P25 (curve 2) and mesoporous TiO_2 powders (curve 3) prepared under the same conditions (except for electrospinning) were also measured. In the absence of catalysts, methylene blue hardly decomposed under UV light irradiation. The photodegradation rate of methylene blue for the TiO_2 hollow fibers was faster than that for P25 and mesoporous TiO_2 powders, so the TiO_2 hollow fibers had good photocatalytic activities for the decomposition of methylene blue. The higher activity might be due to its high BET surface area.

As a common chemical used widely in household products and the chemical industry, formaldehyde is a common environmental pollutant. The elimination of formaldehyde, especially gaseous formaldehyde, in homes is a serious problem.[21] Thus, the decomposition of gaseous formaldehyde by UV light in the presence of TiO_2 hollow fiber as the photocatalyst was used to evaluate the photocatalytic activity of the fibers. Figure 7b shows the change of concentration of formaldehyde gas over time under UV irradiation in the presence of different TiO_2 materials. Control experiments indicated that the photocatalytic reaction hardly proceeded in the absence of TiO_2 (curve 1). After 5 h, up to 42% (curve 2) and 50% (curve 3) of the gaseous formaldehyde was degraded in the presence of Duggusa P25 and mesoporous TiO_2 powders, respectively. For the mesoporous TiO_2 hollow fibers, ca. 80% gaseous formaldehyde was degraded to CO_2 and H_2O under the same conditions (curve 4). The photocatalytic activity of the mesoporous hollow fibers was twice as high as that of commercial P25, possibly because of the increased surface area and photoreactivity of the TiO_2 hollow fibers.[31]

4. Conclusions

Long TiO_2 hollow fibers with mesoporous walls and high surface areas were prepared by the sol−gel two-capillary spinneret electrospinning technique. The mesoporous fibers were as long as 30 cm with diameters of 0.1−4 μm and wall thicknesses of 60−500 nm. The diameter and wall thickness of TiO_2 hollow fibers could be tuned by adjusting the N_2 pressure of the inner and outer capillaries. N_2 adsorption−desorption isotherms gave a BET surface area of 200−208 m^2/g and an average pore size of 6.7 nm. Although the mesopores exhibit 2D hexagonal structure in some area, the arrangement of the nanochannels does not show long-range order. These TiO_2 hollow fibers with mesoporous walls showed higher photocatalytic activities toward decomposition of methylene blue and gaseous formaldehyde than commercial TiO_2 nanoparticles and corresponding mesoporous TiO_2 powders. In addition, the long hollow fibers can be conveniently fixed and reclaimed so they are good candidates for photocatalytic applications.

Acknowledgment. We gratefully acknowledge the financial support of the Doctoral Fund (040422065) of China and the assistance of Dr. Pamela Holt (Shandong University) in manuscript preparation.

Supporting Information Available: Optical photograph of the gel fibers and SEM image of the hollow xerogel fibers, the rheological properties and timed-viscosity curve of the spinnable sol, SEM images of TiO_2 hollow fibers with tunable sizes, the photograph of the xerogel fibers, LA-XRD pattern of xerogel powder, and the photocatalytic-decomposition of methylene blue. This material is available free of charge via the Internet at http://pubs.acs.org.

References and Notes

(1) (a) Hoffmann, M. R.; Martin, S. T.; Choi, W.; Bahnemann, D. W. *Chem. Rev.* **1995**, *95*, 69. (b) Carp, O.; Huisman, C. L.; Reller, A. *Prog. Solid State Chem.* **2004**, *32*, 33. (c) Fujishima, A.; Rao, T. N.; Tryk, D. A. *J. Photochem. Photobiol., C* **2000**, *1*, 1. (d) Sixto, M.; Julián, B.; Alfonso, V.; Christoph, R. *Appl. Catal., B* **2002**, *37*, *1*.

(2) (a) Kasuga, T.; Hiramatsu, M.; Hoson, A.; Sekino, T.; Niihara, K. *Adv. Mater.* **1999**, *11*, 1307. (b) Liu, S. M.; Gan, L. M.; Liu, L. H.; Zhang, W. D.; Zeng, H. C. *Chem. Mater.* **2002**, *14*, 1391. (c) Zhang, L.; Yu, J. C. *Chem. Commun.* **2003**, 2078. (d) Shibata, H.; Ogura, T.; Mukai, T.; Ohkubo, T.; Sakai, H.; Abe, M. *J. Am. Chem. Soc.* **2005**, 127, 16396. (e) Yuan, Z. Y.; Ren, T. Z.; Vantomme, A.; Su, B. L. *Chem. Mater.* **2004**, *16*, 5096.

(3) (a) On, D. T. *Langmuir* **1999**, *15*, 8561. (b) Antonelli, D. M. *Microporous Mesoporous Mater.* **1999**, *30*, 315. (c) Yun, H. S.; Miyazawa, K.; Zhou, H.; Honma, I.; Kuwabara, M. *Adv. Mater.* **2001**, *13*, 1377. (d) Yuan, Z. Y.; Ren, T. Z.; Su, B. L. *Adv. Mater.* **2003**, *15*, 1462. (e) Luo, H.; Wang, C.; Yan, Y. *Chem. Mater.* **2003**, *15*, 3841. (f) Zhou, Y.; Antonietti, M. *J. Am. Chem. Soc.* **2003**, *125*, 14960. (g) Blin, J. L.; Leonard, A.; Yuan, Z. Y.; Gigot, L.; Vantomme, A.; Cheetham, A. K.; Su, B. L. *Angew. Chem., Int. Ed.* **2003**, *42*, 2872.

(4) (a) Coakley, K. M.; Liu, Y.; McGehee, M. D.; Frindell, K. L.; Stucky, G. D. *Adv. Funct. Mater.* **2003**, *13*, 301. (b) Antonielli, D. M.; Ying, J. Y. *Angew. Chem., Int. Ed. Engl.* **1995**, *34*, 2014. (c) Wang, K.; Yao, B.; Morris, M. A.; Holmes, J. D. *Chem. Mater.* **2005**, *17*, 4825. (d) Shibata, H.; Ogura, T.; Mukai, T.; Ohkubo, T.; Sakai, H.; Abe, M. *J. Am. Chem. Soc.* **2005**, *127*, 16396. (e) Kirsch, B. L.; Richman, E. K.; Riley, A. E.; Tolbert, S. H. *J. Phys. Chem. B.* **2004**, *108*, 12698.

(5) Peng, T.; Hasegawa, A.; Qiu, J.; Hirao, K. *Chem. Mater.* **2003**, *15*, 2011.

(6) Mukai, S. R.; Nishihara, H.; Shichi, S.; Tamon, H. *Chem. Mater.* **2004**, *16*, 4987.

(7) Caruso, R. A.; Schattka, J. H.; Greiner, A. *Adv. Mater.* **2001**, *13*, 1577.

(8) (a) Loscertales, I. G.; Barero, A.; Guerrero, I.; Cortijo, R.; Marquez, M.; Ganan-Calvo, A. M. *Science* **2002**, *295*, 1695. (b) Loscertales, I. G.; Barrero, A.; Marquez, M.; Spretz, R.; Velarde-Ortiz, R.; Larson, G. *J. Am. Chem. Soc.* **2004**, *126*, 5376. (c) Larsen, G.; Velarde-Ortiz, R.; Minchow, K.; Barrero, A.; Loscertales, I. G. *J. Am. Chem. Soc.* **2003**, *125*, 1154.

(9) (a) Li, D.; Xia, Y. *Adv. Mater.* **2004**, *16*, 1151. (b) Li, D.; Babel, A.; Jenekhe, S. A.; Xia, Y. *Adv. Mater.* **2004**, *16*, 2062. (c) Li, D.; Wang, Y.; Xia, Y. *Nano Lett.* **2003**, *3*, 1167. (d) McCann, J.; Li, D.; Xia, Y. *J. Mater. Chem.* **2005**, *15*, 735. (e) Xiong, Y.; Mayers, B. T.; Xia, Y. *Chem. Comm.* **2005**, 5013.

(10) (a) Kleitz, F.; Wilezok, U.; Marlow, F. *Phys. Chem. Chem. Phys.* **2001**, *3*, 3486. (b) Marlow, F.; Kleitz, F. *Microporous Mesoporous Mater.* **2001**, *44*, 671.

(11) (a) Lin, H. P.; Mou, C. Y. *Science* **1996**, *273*, 765. (b) Lin, H. P.; Mou, C. Y.; Liu, S. *Adv. Mater.* **2000**, *12*, 103.

(12) (a) Ono, Y.; Nakashima, K.; Sano, M.; Inoue, Y. K.; Hojo, J.; Shinkai, S. *Chem. Commun.* **1998**, 1477. (b) Adachi, M.; Harada, T.; Harada, M. *Langmuir* **2000**, *16*, 2376. (c) Yang, S. M.; Sokolov, I.; Coombs, N.; Kresge, C. T.; Ozin, G. A. *Adv. Mater.* **1999**, *11*, 1427.

(13) (a) Kobayashi, S.; Hnabusa, K.; Hamasaki, N.; Kimura, M.; Shiral, H. *Chem. Mater.* **2000**, *12*, 1523. (b) Caruso, R. A. *Angew. Chem., Int. Ed.* **2004**, *43*, 2746. (c) Miyaji, F.; Davis, S. A.; Charmant, J. P. H.; Mann, S. *Chem. Mater.* **1999**, *11*, 3021.

(14) (a) Martin, C. R. *Science* **1994**, *266*, 1961. (b) Wang, J.; Zhang, J.; Asoo, B. Y.; Stucky, G. D. *J. Am. Chem. Soc.* **2003**, *125*, 13966. (c) Huo, Q.; Zhao, D.; Feng, J.; Weston, K.; Buratto, S. K.; Stucky, G. D. *Adv. Mater.* **1997**, *9*, 974. (d) Miyata, H.; Kuroda, K. *Adv. Mater.* **2001**, *13*, 558. (e) Soler-lllia, G. J. de A. A.; Sanchez, C.; Lebeau, B.; Patarin, J. *Chem. Rev.* **2002**, *102*, 4093. (f) Xiong, C.; Balkus, K. J., Jr. *Chem. Mater.* **2005**, *17*, 5136.

(15) (a) Doshi, J.; Reneker, D. H. *J. Electrost.* **1995**, *35*, 151. (b) Reneker, D. H.; Chun, I. *Nanotechnology* **1996**, *7*, 216. (c) Dzenis, Y. *Science* **2004**, *304*, 1917. (d) Zhang, Y.; Huang, Z. M.; Xu, X.; Lim, C. T.; Ramakrishna, S. *Chem. Mater.* **2004**, *16*, 3406. (e) Jayasinghe, S. N.; Sullivan, A. C. *J. Phys. Chem. B.* **2006**, *110*, 2522.

(16) (a) Katta, P.; Alessandro, M.; Ramsier, R. D.; Chase, G. G. *Nano Lett.* **2004**, *4*, 2215. (b) Bognitzki, M.; Czado, W.; Frese, T.; Schaper, A.; Hellwig, M.; Steinhart, M.; Greiner, A.; Wendorff, J. H. *Adv. Mater.* **2001**, *13*, 70. (c) Li, D.; Xia, Y. *Nano* Lett. **2003**, *3*, 555. (d) Li, D.; Ouyang, G.; McCann, J.; Xia, Y. *Nano Lett.* **2005**, *5*, 913.

(17) (a) Madhugiri, S.; Sun, B.; Smirniotis, P. G.; Feraris, J. P.; Balkus, K. J., Jr. *Microporous Mesoporous Mater.* **2004**, *69*, 77. (b) Madhugiri, S.; Dalton, A.; Gutierrez, J.; Ferraris, J. P.; Balkus, K. J., Jr. *J. Am. Chem. Soc.* **2003**, *125*, 14531. (c) Yu, J. H.; Fridrikh, S. V.; Rutledge, G. C. *Adv. Mater.* **2004**, *16*, 1562. (d) Madhugiri, S.; Zhou, W.; Ferraris, J. P.; Balkus, K. J., Jr. *Microporous Mesoporous Mater.* **2003**, *63*, 75.

(18) (a) Dersch, R.; Liu, T.; Schaper, A. K.; Greiner, A.; Wendorff, J. H. *J. Polym. Sci. Part A: Polym. Chem.* **2003**, *41*, 545. (b) Dersch, R.; Steinhart, M.; Boudriot, U.; Greiner, A.; Wendorff, J. H. *Polym. Adv. Technol.* **2005**, *16*, 276. (c) Sun, Z.; Zussman, E.; Yarin, A. L.; Wendorff, J. H.; Greiner, A. *Adv. Mater.* **2003**, *15*, 1929.

(19) (a) Lee, S.; Sheridan, M.; Mills, A. *Chem. Mater.* **2005**, *17*, 2744. (b) Stathatos, E.; Petrova, T.; Lianos, P. *Langmuir* **2001**, *17*, 5025.

(20) (a) Zhang, L.; Zhu, Y.; He, Y.; Li, W.; Sun, H. *Appl. Catal., B* **2003**, *40*, 287. (b) Shang, J.; Yao, W.; Zhu, Y.; Wu, N. *Appl. Catal., A* **2004**, *257*, 25. (c) Shang, J.; Li, W.; Zhu, Y. *J. Mol. Catal., A* **2003**, *202*, 187.

(21) Wang, C.; Rabani, J.; Bahnemann, D. W.; Dohrmann, J. K. *J. Photochem. Photobiol., A* **2002**, *148*, 169.

(22) (a) Yang, P.; Zhao, D.; Chmelka, B. F.; Stucky, G. D. *Chem. Mater.* **1998**, *10*, 2033. (b) Soler-Illia, G. J. de A. A.; Crepaldi, E. L.; Grosso, D.; Sanchez, C. *Curr. Opin. Colloid Interface Sci.* **2003**, *8*, 109. (c) Grosso, D.; Cagnol F.; Soler-Illia, G. J. de A. A.; Crepaldi, E. L.; Amenitsch, H.; Brunet-Bruneau, A.; Bourgeois, A.; Sanchez, C. *Adv. Funct. Mater.* **2004**, *14*, 309. (d) Grosso, D.; Soler-Illia, G. J. de A. A.; Babonneau, F.; Sanchez, C.; Albouy, P.; Brunet-Bruneau, A.; Balkenende, A. R. *Adv. Mater.* **2001**, *13*, 1085. (e) Grosso, D.; Balkenende, A. R.; Albouy, P. A.; Ayral, A.; Amenitsch, H.; Babonneau, F. *Chem. Mater.* **2001**, *13*, 1848. (f) Brinker, C. J.; Lu, Y.; Sellinger, A.; Fan, H. *Adv. Mater.* **1999**, *11*, 579.

(23) Jung, K. T.; Chu, Y. H.; Haam, S.; Shul, Y. G. *J. Non-Cryst. Solids* **2002**, *298*, 193.

(24) (a) Alberius, P. C. A.; Frindell, K. L.; Hayward, R. C.; Kramer, E. J.; Stucky, G. D.; Chmelka, B. F. *Chem. Mater.* **2002**, *14*, 3284. (b) Yang, P.; Zhao, D.; Margolese, D. I.; Chmelka, B. F.; Stucky, G. D. *Chem. Mater.* **1999,** *11*, 2813. (c) Andersson, M.; Birkedal, H.; Franklin, N. R.; Ostomel, T.; Boettcher, S.; Palmqvist, A. E. C.; Stucky, G. D. *Chem. Mater.* **2005**, *17*, 1409. (d) Yu, J. C.; Wang, X.; Fu, X. *Chem. Mater.* **2004**, *16*, 1523.

(25) (a) Lu, Q.; Chen, D.; Jiao, X. *Chem. Mater.* **2005**, *17*, 4168. (b) Gross, A. F.; Le, V. H.; Kirsch, B. L.; Riley, A. E.; Tolbert, S. H. *Chem. Mater.* **2001**, *13*, 3571. (c) Blin, J. L.; Léonard, A.; Su B. L. *J. Phys. Chem. B* **2001**, *105*, 6070. (d) Calleja, G.; Serrano, D. P.; Sanz, R.; Pizarro, P.; Garcia, A. *Ind. Eng. Chem. Res.* **2004**, *43*, 2485.

(26) (a) Yue, Y.; Gao, Z. *Chem. Commun.* **2000**, 1755. (b) Yang, P.; Zhao, D.; Margolese, D. I.; Chmelka, B. F.; Stucky, G. D. *Nature* **1998**, *396*, 152.

(27) (a) Corma, A. *Chem. Rev.* **1997**, *97*, 2373. (b) Tolbert, S. H.; Schaffer, T. E.; Feng, J.; Hansma, P. K.; Stucky, G. D. *Chem. Mater.* **1997**, *9*, 1962.

(28) (a) Beyers, E.; Cool, P.; Vansant, E. F. *J. Phys. Chem. B* **2005**, *109*, 10081. (b) Yu, J. C.; Zhang, L.; Yu, J. *Chem. Mater.* **2002**, *14*, 4647. (c) Yu, J. C.; Ho, W.; Yu, J.; Hark, S. K.; Iu, K. *Langmuir* **2003**, *19*, 3889. (d) Sreethawong, T.; Suzuki, Y.; Yoshikawa, S. *J. Solid State Chem.* **2005**, *178*, 329. (e) Zhang, C.; Zhu, Y. *Chem. Mater.* **2005**, *17*, 3537.

(29) (a) Butterfield, I. M.; Christensen, P. A.; Hamnett, A. *J. Appl. Electrochem.* **1997**, *27*, 385. (b) Chen, J.; Rulkens, W. H.; Bruning, H. *Water Sci. Technol.* **1997**, *35*, 231. (c) Sopyan, I.; Watanabe, M.; Murasawa, S.; Hashimoto, K.; Fujishima, A. *J. Photochem. Photobiol., A* **1996**, *98*, 79. (d) Zhu, Y.; Zhang, L.; Wang, L.; Fu, Y.; Cao, L. *J. Mater. Chem.* **2001**, *11*, 1864. (e) Zhu, Y.; Zhang, L.; Yao, W.; Cao, L. *Appl. Surf. Sci.* **2000**, *158*, 32.

(30) (a) Gole, J. L.; Stout, J. D.; Burda, C.; Lou, Y.; Chen, X. *J. Phys. Chem. B* **2004**, *108*, 1230. (b) Nagaveni, K.; Hegde, M. S.; Ravishankar, N.; Subbanna, G. N.; Madras, G. *Langmuir* **2004**, *20*, 2900.

(31) (a) Wang, X.; Yu, J.; Ho, C.; Hou, Y.; Fu, X. *Langmuir* **2005**, *21*, 2552. (b) Sinha, A. K.; Suzuki, K. *J. Phys. Chem. B* **2005**, *109*, 1708. (c) Fetterolf, M. L.; Patel, H. V.; Jennings, J. M. *J. Chem. Eng. Data* **2003**, *48*, 831.